Elasticity Size Effects in ZnO Nanowires-A Combined Experimental-Computational Approach

ARTICLE *in* NANO LETTERS · NOVEMBER 2008

Impact Factor: 13.59 · DOI: 10.1021/nl801724b · Source: PubMed

4 AUTHORS, INCLUDING:

Ravi Agrawal
Shell Technology Centre Bangalore
14 PUBLICATIONS **565** CITATIONS
SEE PROFILE

Horacio Dante Espinosa
Northwestern University
162 PUBLICATIONS **4,048** CITATIONS
SEE PROFILE

NANO LETTERS

Letter

Elasticity Size Effects in ZnO Nanowires#A Combined Experimental-Computational Approach

Ravi Agrawal, Bei Peng, Eleftherios E. Gdoutos, and Horacio D. Espinosa

Nano Lett., **2008**, 8 (11), 3668-3674 • DOI: 10.1021/nl801724b • Publication Date (Web): 08 October 2008

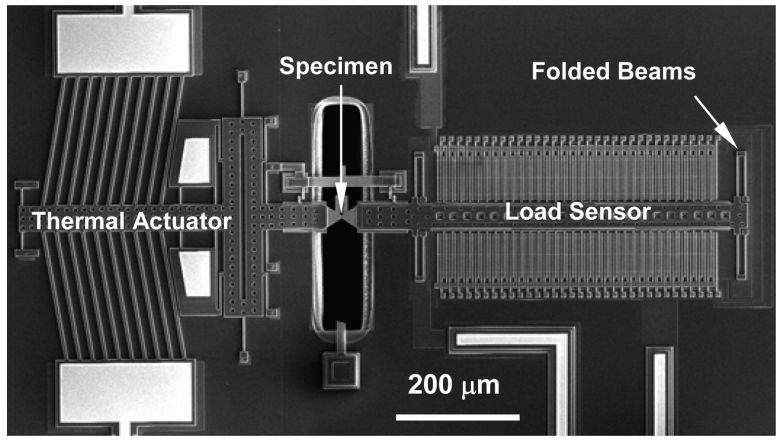

More About This Article

Additional resources and features associated with this article are available within the HTML version:

- Supporting Information
- Access to high resolution figures
- Links to articles and content related to this article
- Copyright permission to reproduce figures and/or text from this article

View the Full Text HTML

Nano Letters is published by the American Chemical Society. 1155 Sixteenth Street N.W., Washington, DC 20036

NANO LETTERS

2008
Vol. 8, No. 11
3668-3674

Elasticity Size Effects in ZnO Nanowires—A Combined Experimental-Computational Approach

Ravi Agrawal,† Bei Peng,† Eleftherios E. Gdoutos, and Horacio D. Espinosa*

Department of Mechanical Engineering, 2145 Sheridan Road, Northwestern University, Evanston, Illinois 60208-3111

Received June 16, 2008; Revised Manuscript Received August 19, 2008

ABSTRACT

Understanding the mechanical properties of nanowires made of semiconducting materials is central to their application in nano devices. This work presents an experimental and computational approach to unambiguously quantify size effects on the Young's modulus, *E*, of ZnO nanowires and interpret the origin of the scaling. A micromechanical system (MEMS) based nanoscale material testing system is used in situ a transmission electron microscope to measure the Young's modulus of [0001] oriented ZnO nanowires as a function of wire diameter. It is found that *E* increases from ~140 to 160 GPa as the nanowire diameter decreases from 80 to 20 nm. For larger wires, a Young's modulus of ~140 GPa, consistent with the modulus of bulk ZnO, is observed. Molecular dynamics simulations are carried out to model ZnO nanowires of diameters up to 20 nm. The computational results demonstrate similar size dependence, complementing the experimental findings, and reveal that the observed size effect is an outcome of surface reconstruction together with long-range ionic interactions.

The semiconductive, piezoelectric, and biocompatible properties of zinc oxide (ZnO) nanostructures have attracted the attention of many scientists and engineers, eager to implement this novel material into high-power optoelectronic devices,[1] logic circuits,[2] piezoelectric devices,[3] nanoresonators, and electromechanically coupled nanocantilever sensors.[4] At the nanoscale, the dependence of material properties on size and shape becomes a crucial factor in designing such devices with predictable and reproducible operation. The small dimensions of the nanostructures, however, raise serious challenges for the experimental investigation of properties relevant to the applications of the device.

A variety of experimental techniques have been developed to measure the mechanical properties of individual ZnO nanostructures. However, the elastic modulus of [0001] oriented ZnO nanowires (NWs) reported so far ranges from 20 to 250 GPa with no consensus on the value for a particular wire diameter. This is in particular troublesome but not unexpected given the challenges in identifying nanoscale mechanical properties. The discrepancies appear to be due to differences in the experimental protocols and errors associated with each technique. To provide needed background, we next summarize some of the previously employed testing techniques, their results, and limitations. A popular nanomechanical testing technique is based on the analysis of the dynamic response of a NW cantilever when subjected to an alternating electrostatic field of known frequency inside a transmission electron microscope (TEM). The Young's modulus of the NW is calculated from the amplitude and phase of the dynamic response caused by the applied field.[5−7] The effective Young's modulus found using this technique increased from 140 to 220 GPa as the wire diameter decreased from 120 to 17 nm.[7] This technique provides direct visualization of the experiment and avoids the need for specimen manipulation, but the deformation is essentially gradient-dominated which has a more pronounced surface elasticity effect than axial monotonic deformation.[7] Other techniques based on atomic force microscopy (AFM) have also been employed. A size independent Young's modulus of (38.2 ± 1.8) GPa was measured by a three-point bending AFM test[8] for ZnO nanobelts in the thickness range of 50−140 nm. In single clamped NW bending experiments,[9] using an AFM, a value of (29 ± 8) GPa was identified. By contrast, using a contact resonance AFM technique, values of 104−198 GPa were measured for wires ranging from 25.5 to 134.4 nm in diameter.[10] The reader should note that several of the reported measurements fall below the modulus measured in bulk single crystals, which is ~140 GPa in the [0001] direction.[11] Therefore, one wonders if this is a physical effect or the result of experimental artifacts.

AFM-based techniques have adequate force and displacement resolution, but lack in situ real time imaging capabilities and, therefore, are prone to uncertainties in data interpretation. For example, it is difficult to precisely measure the

* To whom correspondence should be addressed. Phone: (847) 467-5989. Fax: (847) 491-3915. E-mail: espinosa@northwestern.edu.

† These authors contributed equally to this work.

10.1021/nl801724b CCC: $40.75
Published on Web 10/08/2008

contact area between AFM tip and the NW in contact resonance tests as adhesion forces become significant at such scales. Also the AFM-based nanoindentation technique is sensitive to substrate effects for small diameter nanowires.[10] The compounded error introduced by these effects may explain why the elastic modulus of a 250 nm × 450 nm nanobelt was calculated to be 100 GPa, which is significantly lower than the modulus measured in bulk crystals of 140 GPa.[11] In addition to these AFM-based techniques, tensile tests with a microfabricated test stage[12] or a piezoelectric nanomanipulator[13] have also been used for the mechanical characterization of a ZnO NWs. These techniques enable uniaxial in situ experiments inside a scanning electron microscope (SEM) but require that the test stage be accurately calibrated and the specimen properly manipulated and fixed. Desai et al. measured a very low Young's modulus of 21.1 GPa for a ZnO NW 287 nm in diameter, probably due to errors introduced by loading a compliant SiO_2 grid with the NW attached to it instead of loading the NW directly.[12] Another possible source of error arises from the limited strength of the welds at the specimen ends. Hoffmann et al. claimed that carbon deposition is strong enough to make a firm bond between NW and nanomanipulator.[12] However, we found that carbon deposition results in weld slippage, when loading NWs with diameters larger than 200 nm (see Supporting Information for details). From a thorough study of the literature, we concluded that the procedures used in mounting and fixing the specimens to the loading stage may adversely affect the interpretation and accuracy of the results.

Apart from the inconsistency in reported values for Young's modulus, there is also an ambiguity about the size dependence. Some of the studies discussed above report a size dependence in ZnO NWs with diameters smaller than 150[7] or 80 nm,[10] while others report no specific size dependence.[8,9,12] To explain the size-dependence in their studies, Chen et al.[7] proposed a core−shell model, where the NW is treated as a composite with a shell and a core structure. This model is based on fitting the experimental data and assumes a core with bulk's Young's modulus and a shell with higher modulus. The limitation of this model comes from the limited size range studied in the experiments. From data fitting, the shell thickness turns out to be the radius of the smallest NW in the experimentally studied regime and the shell modulus is the modulus of this smallest NW.[10] This highlights the need for atomistic studies to assess the validity and accuracy of the core−shell model. Computationally, nanobelts of various axial orientations have been studied using MD simulations,[14] although the biggest size modeled was ∼4.5 nm. Size dependence was observed for [0001] oriented nanobelts, but convergence to the bulk Young's modulus was reported for a nanobelt with lateral dimension of 4.5 nm. This is in direct conflict with experimental measurements as size effect has been reported to exist well beyond 4.5 nm and up to ∼100 nm. In a recent paper,[15] the same researchers rectified their conclusions and reported that the size effect exists beyond a critical dimension of 4.5 nm; however, the largest wire studied was still smaller than 5.0 nm.

In summary, a detailed review of the literature reveals lack of agreement in experimentally measured mechanical properties and modeling predictions. The discrepancy is directly related to uncertainties in (i) NW diameter or cross-sectional area, (ii) boundary and loading conditions, (iii) calibration of the instruments, and (iv) the way samples are mounted and fixed. From a computational standpoint, the sizes modeled were too small, and therefore a big gap exists between computationally and experimentally studied nanowires. Furthermore, to the best of our knowledge, there is no fundamental explanation for the observed size dependence other than the generally invoked surface to volume ratio.

The conflicting reports on Young's modulus and its dependence on wire diameter motivated the development of an accurate testing technique and a thorough atomistic study of the elastic properties of ZnO NWs. In this paper, we present a quantitative in situ TEM tensile testing technique to measure the mechanical properties of ZnO NWs with lateral dimensions in the range of 20−400 nm. The nanoscale material testing system (n-MTS) consists of a miniaturized testing stage based on MEMS technology.[16−18] Molecular dynamics (MD) simulations for NWs with diameters between 5 and 20 nm are also carried out to complement the experimental findings. This combined experimental and computational approach resolves the existing controversy and provides a fundamental understanding of the observed elasticity size effect.

In the MEMS-based n-MTS system,[16−19] load is applied using a thermal actuator on one side of the testing stage, and displacement is measured using a differential capacitive sensor on the other side[20] (see Figure 1a). The force-displacement response of individual ZnO NW was measured electronically with simultaneous observation of their atomic structure in real time during the loading process. One of the key advantages of this technique is the uniaxial state of loading, which eliminates many sources of experimental error, simplifies the analysis of results, and makes experiments more amenable to modeling with minimal assumptions. The ZnO NW samples used for these experiments were obtained from NanoLab, Inc. The NWs were high quality single crystals having a [0001] oriented wurtzite structure with lattice constants $a = 3.25$ Å and $c = 5.20$ Å [21] and typical lengths between 5 and 10 μm. Twelve NWs with diameters ranging from 20.4 to 412.9 nm were tested and their Young's modulus experimentally measured.

The ZnO NWs were first dispersed in isopropyl alcohol, by ultrasonication for 1 min, and then poured on a copper TEM grid, letting the alcohol to evaporate leaving behind the NWs on the grid. A NW was then chosen, based on its diameter and length, and transported to the testing stage using a piezoelectric nanomanipulator built by Klocke Nanotechnik.[22] The mounting process was performed inside a FEI NOVA600 SEM and the NW was attached to the testing stage by e-beam induced deposition of Pt at both ends.[17,18] Figure 1b shows a NW mounted on the device. The testing stage[22] with a NW mounted on it was placed on a specially designed TEM holder.[23] The specimen was then loaded incrementally until failure was detected by significant

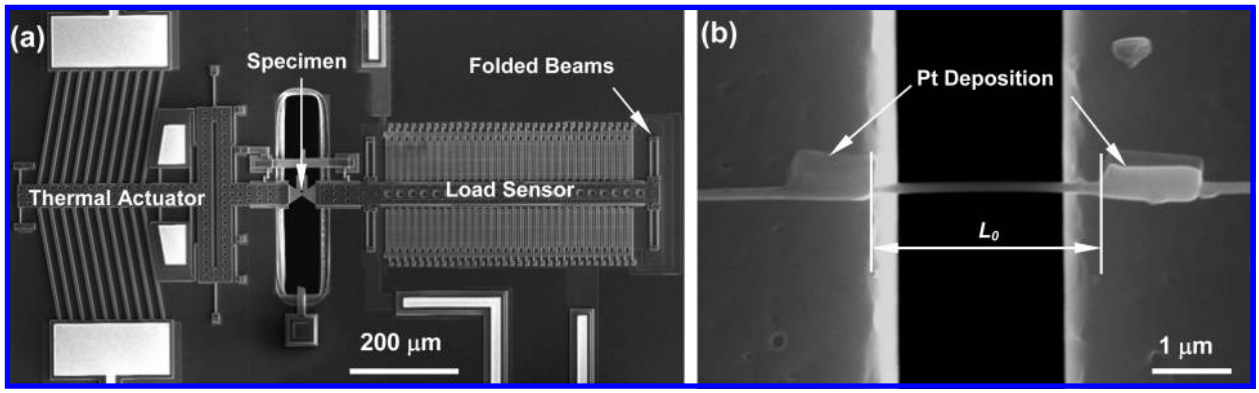

Figure 1. (a) SEM micrograph of microelectromechanical system used to test nanowires in situ a transmission electron microscope. (b) NW specimen suspended between thermal actuator and load sensor. Specimen ends were welded to the testing system by electron beam induced deposition of platinum.

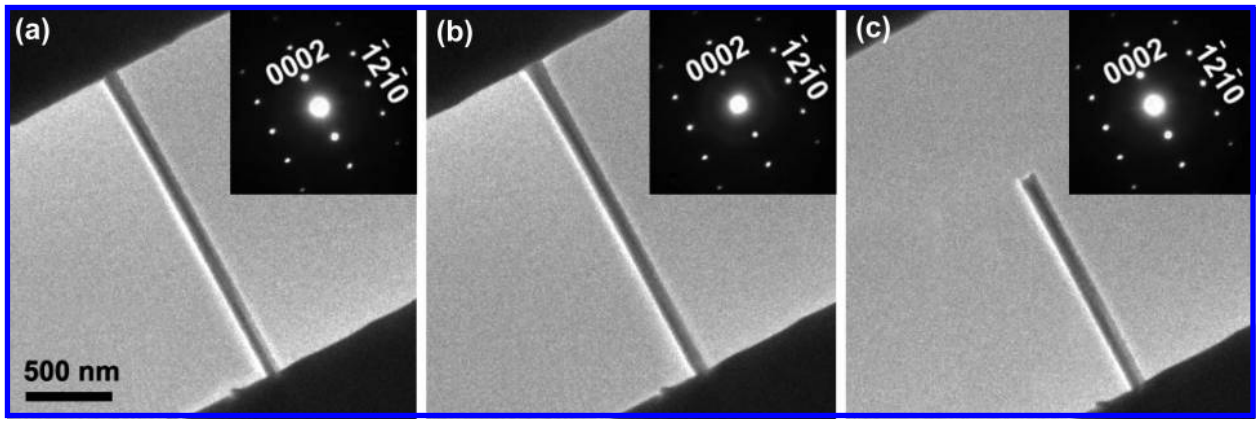

Figure 2. TEM images of a ZnO nanowire at various stages in the tensile testing: (a) before loading, (b) at ~2.5% strain, (c) after failure. The insets are selected area diffraction patterns taken at each loading state.

decrease in load and/or by visual identification of fracture. TEM images and selective area diffraction (SAD) patterns were taken during the loading at different strain levels. Figure 2 shows TEM images of the specimen taken during a tensile loading experiment: (a) prior to loading; (b) at ~2.5% strain and (c) after failure. In the insets of Figure 2a−c, the corresponding SAD patterns are shown. In order to calculate Young's modulus, strains and corresponding stresses were calculated as described next.

Strains were calculated in two independent ways to verify absence of slippage at the fixed ends of the NW: (i) average strains based on the overall length of the NW; (ii) local atomic strains from SAD patterns. For the average strain, the NW elongation, ΔL, was assumed to be the same as the increase of the gap size of the testing stage and extracted from the TEM images. The average strain was then computed as $\Delta L/L_0$, where L_0 is the initial gap at 0% strain. For local atomic strains, intensity profiles along the c-axis in the SAD patterns were analyzed. In Figure 3a, intensity profiles obtained from the SAD patterns (Figure 2a and Figure 2b, respectively) are plotted. The three peaks in the profile correspond to the $(000\bar{2})$, (0000), and (0002) planes. The change in plane spacing is then calculated by $\Delta c = \delta c^2/(2 - \delta c)$ where δ is the peak shift (shown in Figure 3a) and c is the lattice spacing at 0% strain. The local atomic strain was then computed as $\Delta c/c$. For calculation of stresses, forces were obtained from the calibration of the load sensor[17] with an uncertainty of 2% and cross-sectional areas were determined by analyzing the fractured surface of the NWs. After the test, the fractured NWs were again attached to the nanomanipulator tungsten tip and placed inside a field emission SEM so as to image the cross-section (inset of Figure 3b). The cross-section of the NWs was observed to be hexagonal, although not with all sides equal. Note that the hexagonal geometry of the cross-section is contrary to the circular one reported by Stan et al.[10] With all the necessary quantities measured (strains, forces, and cross-sectional areas), stress−strain signatures were computed for each of the tested NWs.

Figure 3b shows the stress−strain response of one of the specimens. For this case, the initial length (L_0), was measured to be 2.63 ± 0.002 μm. Using the two methods of calculating strain, the Young's modulus was found to be 136.5 and 140.8 GPa, respectively. The small (<4%) difference between the two methods confirms that there was no slippage between the NW and the testing stage when fixed via Pt deposition. Measured values of Young's modulus values, as a function of wire diameters, are plotted in Figure 4a. The experimental

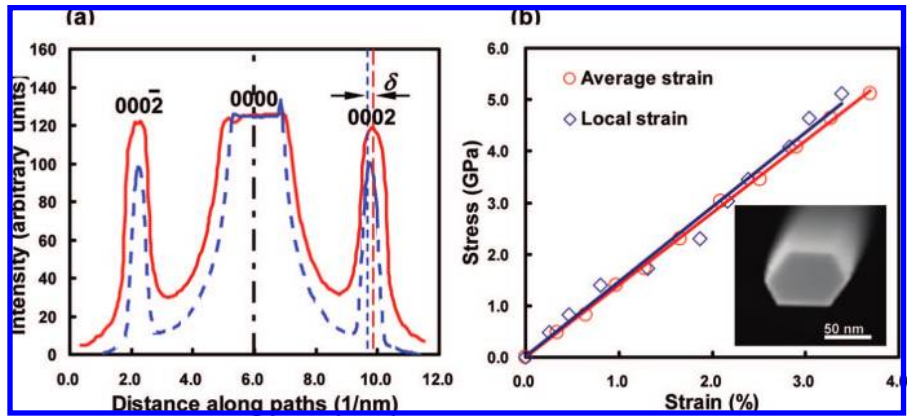

Figure 3. (a) Intensity profiles of SAD patterns for a NW prior to loading (solid line) and at ~2.5% strain (dashed line). (b) Stress−strain curves computed from average displacements and lattice spacing in reciprocal space obtained from SAD images. The inset shows the cross-section of the NW as imaged by scanning electron microscopy.

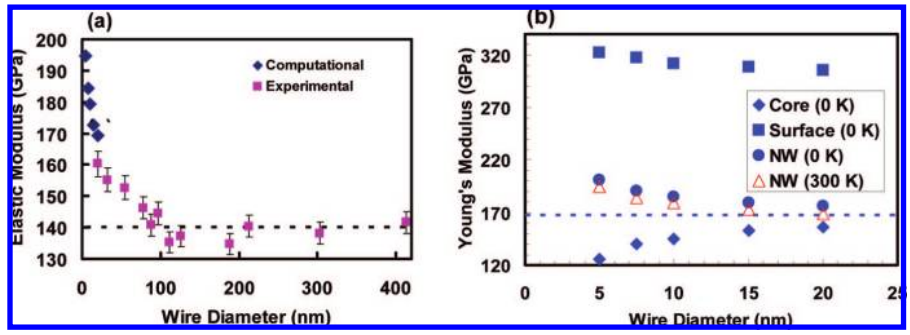

Figure 4. (a) Variation of Young's modulus with wire diameter (the dashed line shows the experimentally reported bulk value of ~140 GPa). (b) Computational results showing the variation of Elastic modulus with wire size at 0 K and 300 K. The individual contribution from the outermost shell atoms and rest of the core atoms is also shown at 0 K.

data reveals that a significant size dependence of the Young's modulus for [0001] oriented ZnO NWs exists when the wire diameter is smaller than ~100 nm. For larger diameters, the Young's modulus is found to be approximately the bulk value of 140 GPa.[11] To gain a fundamental understanding of the size dependence observed in the experiments, we simulated atomistically the tensile behavior of ZnO nanowires with diameters ranging from 5 to 20 nm.

Modeling of [0001] oriented ZnO NWs was carried out with LAMMPS (large-scale atomic/molecular massively parallel simulator),[24,25] developed at Sandia National Laboratories. The atomic interactions were modeled with a Buckingham type potential of the following form:

$$E_{\text{total}}(r_{ij}) = \sum_{i=1}^{N}\sum_{j\neq i} A\exp\left(-\frac{r_{ij}}{\rho}\right) - \frac{C}{r_{ij}^6} + E_{\text{long}}(r_{ij}) \qquad (1)$$

where r_{ij} is the distance between two atoms in a cell, A, C, and ρ are parameters defining the short-range interactions and $E_{\text{long}}(r_{ij})$ represents the long-range electrostatic interactions based on the ionic charge. The Buckingham potential has been used successfully to predict crystal properties such as lattice energies and lattice spacing[26] for selected values of A, C, and ρ. The constants identified by Binks[26] were used in the calculations. Short-range interactions between atoms more than 8.5 Å apart were ignored.[26] In this study, the long-range interactions were calculated based on the summation proposed by Wolf et al.[27]

$$E_{\text{long}}(r_{ij}) = \frac{1}{2}\sum_{i=1}^{N}\sum_{\substack{j\neq i \\ (r_{ij}<R_c)}}\left(\frac{q_i q_j erfc(\alpha r_{ij})}{r_{ij}} - \lim_{r_{ij}\to R_c}\left\{\frac{q_i q_j erfc(\alpha R_c)}{r_{ij}}\right\}\right) - \left(\frac{erfc(\alpha R_c)}{2R_c} + \frac{\alpha}{\sqrt{\pi}}\right)\sum_{i=1}^{N} q_i^2 \qquad (2)$$

where q_i and q_j are the ionic charges. In the above formula, R_c is a quasi-cutoff radius proportional to computational time, and α is a damping coefficient. On the basis of convergence studies detailed in Supporting Information, $R_c = 7$ Å and $\alpha = 0.4$. The Wolf summation for calculating long-range interactions is computationally more efficient and does not require periodic boundary conditions to be imposed on the cell, as it is the case in the traditionally used Ewald summation.[27] We note that the computational efficiency of the Wolf summation and its ability to model free surfaces allowed the simulation of wires with diameters approaching those experimentally tested. As a result, a link between theory and experiments was achieved.

Hexagonal cross-sectional wires were modeled with lateral dimensions ranging from 5 to 20 nm. Periodic boundary conditions were imposed in the axial ([0001]) direction effectively extending the wire to infinity in that direction. An aspect ratio of ~3:1 was maintained for all simulated

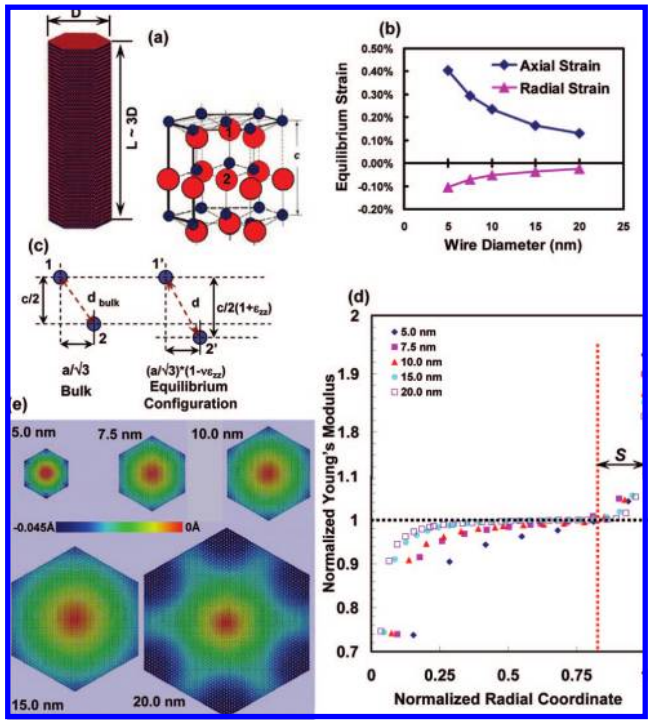

Figure 5. (a) Atomic model of [0001] oriented ZnO nanowire prior to annealing along with the wurtzite crystal structure. (b) Equilibrium axial strain, observed at 0 K, after minimization for nanowires of different diameters. (c) A schematic diagram showing the calculation of effective interatomic distance based on axial and transverse strains. (d) Young's modulus normalized by the bulk value in each atomic layer of the wire cross section. (e) Contour of radial displacements, for nanowires of different diameters, upon surface relaxation.

NWs. Figure 5a shows the atomic model for a 7.5 nm wire prior to annealing. An annealing process was simulated to mimic the manufacturing process, where O^{2-} infuses into zinc powder in a furnace at approximately 1100 K.[28] The temperature of the NWs was raised to 1200 K within 30 ps and then equilibrated for 30 ps. The wires were then cooled down to 300 K (room temperature) in 30 ps and equilibrated for another 30 ps. NPT conditions using the Nose−Hoover thermostat were imposed in these processes.[24] A time frame of 30 ps was found to be long enough for the energy and pressure of the NWs to stabilize at the specified temperature. Following the annealing process, a quasi-static loading scheme was employed to simulate the room temperature loading process. This happened in two steps: (1) the structure was deformed in 0.5% strain steps over a period of 1 ps under NVT conditions, and (2) the structure was allowed to relax at each strain level under NPT conditions for 30 ps. An average over 2 ps at the end of the relaxation process is used to obtain the atomic coordinates at various strain levels. The virial stresses[24] were calculated for each level of strain and the Young's modulus was found from the slope of the elastic region of the stress−strain curve.

A size dependence following the same trend as the one identified experimentally was found. The Young's modulus increased from 169 to 194 GPa as wire diameter decreased from 20 to 5 nm. The computational and experimental

Table 1. Measured and Computed Young's Modulus of Nanowires with Different Diameters

method	outer diameter (nm)	length (mm)	Young's modulus (GPa)
Computational	5	Periodic (0.015)	194.6
	7.5	Periodic (0.022)	184.3
	10	Periodic (0.030)	179.3
	15	Periodic (0.045)	172.6
	20	Periodic (0.052)	169.2
Experimental	20.4	1.34	160.3
	32.2	1.53	155.2
	54.9	1.01	152.7
	77.5	1.45	146.3
	88.2	2.63	140.8
	96.7	4.32	144.5
	111	2.01	135.4
	125.9	2.98	137.3
	188.5	3.57	134.8
	212.6	2.55	140.4
	303.2	3.01	138.2
	412.9	3.11	141.6

findings are summarized together in Table 1 and the Young's modulus as a function of NW diameter is plotted in Figure 4a. As expected, no convergence to the bulk value was observed in the computationally studied range. For the largest modeled NW, corresponding to the smallest tested wire, a Young's modulus of 169 GPa was computed, which is in general good agreement with the modulus of 160.9 GPa experimentally measured for a 20.4 nm wire. The difference can in part be attributed to the fact that the MD force field overestimates the bulk Young's modulus with a value of 157 GPa, as opposed to the experimentally measured 140 GPa.[11]

To analyze the origin of the size dependence, the atomic rearrangement due to surface effects was examined. The lattice spacing and intrinsic strains of different sized wires were analyzed after initial minimization at 0 K, to remove the affect of thermal vibrations of atoms at room temperature. It was observed that the wire surfaces were initially under compression along the wire axis. After minimization, an equilibrium configuration was attained with the compressive surface stresses being balanced by tensile stresses in the center of the wire. Overall, the nanowires expanded in the axial direction and the axial strain at equilibrium decayed with increasing wire size approaching zero strain for large wire diameters. Due to Poisson's effect, a corresponding radial contraction of the wire was also observed. Figure 5b shows the axial and radial strains in the minimized states for wires of different sizes.

Building upon the idea of the core−shell model proposed earlier,[7] we obtained from the simulations the Young's modulus of the different atomic layers in the cross section of the NWs. We observed that the surface atoms exhibited a Young's modulus much higher than the bulk value and that exhibited by the inner atoms, which is in overall agreement with the core−shell model. Figure 4b shows the contribution of the surface atoms and the remaining atoms to the overall Young's modulus of the NWs. Interestingly, because of the overall wire expansion, one is at first puzzled by such result. In fact, for a simple spring-mass model,[29] where the spring force field is modeled as electrostatic

interaction, the dominant interaction in ionic compounds, it is easy to show that the elastic modulus E is inversely proportionally to the interatomic spacing d to the fourth power; that is, $E \propto d^{-4}$. Hence, d for the surface atoms should be smaller than the bulk interatomic spacing even in the presence of an overall axial expansion of the NW as predicted by energy minimization. The computational result depicted in Figure 4 can be explained by examining the local rearrangement of atoms and bond length from which interatomic forces are computed, rather than the c-axis lattice spacing in isolation. From the simulations, it was found that surface reconstruction causes not only an increase in the [0001] interatomic spacing but also a radial inward contraction. Figure 5c schematically shows how the effective bond length is affected by both axial and radial strains. For example, the effective interatomic spacing between Zn^{2+} ions 1 and 2 (as shown in Figure 5c) can be calculated using the following equation:

$$d = \sqrt{\left(\frac{c^2(1+\varepsilon)^2}{4}\right) + \left(\frac{a^2(1-\nu\varepsilon)^2}{3}\right)}$$

where c is the bulk lattice spacing along the c-axis, a is the other lattice coordinate, ε is the local axial strain and ν is the local Poisson's ratio. For a strain free bulk crystal, $\varepsilon = 0$ and $d_{bulk} = [(c^2/4) + (a^2/3)]^{1/2}$. For a NW at equilibrium with tensile axial strain induced by surface relaxation (i.e., $\varepsilon > 0$), d is always greater than d_{bulk} unless the local Poisson's ratio increases beyond a critical value ($\sim$1.8 for observed equilibrium strains in our simulations). Locally on the surface of the wires, ν was found sufficiently high to make the effective interatomic spacing of the surface atoms smaller than that of bulk by $\sim$11%. A bond length contraction of 11% on the surface yields a Young's modulus of $\sim$270 GPa for the outermost shell, which is higher than the modulus of the bulk ($\sim$167 GPa at 0 K), as predicted by the Buckingham potential. This qualitatively explains that the higher Young's modulus associated with surface atoms is due to local rearrangement of atoms leading to a decrease in the effective interatomic spacing. Contribution of individual layers of atoms of the NW to its overall Young's modulus is shown in Figure 5d in normalized coordinates. It can be seen that the effect of surface reconstruction rapidly decays beyond a certain number of atomic layers, and the number of these atomic layers increases as the wires size increases. Quantitatively, an effective shell thickness can be defined as a region in which the elastic modulus is greater than the bulk value. Using this definition, Figure 5d, the shell thickness was found to be $\sim$15% of the wire diameter. Note that the shell thickness is not constant for all wire sizes, in contrast to the assumption made in the core−shell model.[7,10] The dependence of shell thickness on the wire size can be attributed to long-range electrostatic interactions. Also the atoms in the core region do not exhibit bulk properties as assumed in the core−shell model (see Figure 5d). They exhibit a softer behavior, which is more pronounced as the wire diameter decreases. Figure 5e shows the radial displacements of the atoms along the cross section for nanowires of different sizes, as observed in the minimized configurations. Blue atoms (closer to the surface of the NWs) represent the region with high radial strains in which the effect of surface relaxation is more pronounced. The larger blue zones suggest a more distributed surface effect on radial strains, which makes the surface atoms less stiff for a larger wire (see Figure 4b). The higher Young's modulus of the surface atoms together with increasing surface to volume ratios, results in small size wires having a higher Young's modulus. A similar behavior is expected at 300 K, as we observe a similar trend in Young's modulus with increasing wire size. Temperature shifts down the Young's modulus versus diameter curve (as shown in Figure 4b), which is consistent with the above reasoning as higher temperature results in a thermal expansion and therefore a larger interatomic spacing.

In this work, the size effect of Young's modulus of ZnO NWs was investigated experimentally as well as computationally. Experimentally, ZnO NWs with diameters ranging from 20.4 to 412.9 nm were tested under a uniaxial tensile load using a nanoscale materials testing system inside a TEM. Uncertainties in measuring the cross-sectional area were avoided by imaging the fractured cross-section with a high resolution SEM. Computation of strains based on nanodiffraction (SAD) confirmed that platinum welds are strong enough to prevent any wire slippage. The study proved unambiguously that the Young's modulus of ZnO NWs monotonically decreases from 160 to 140 GPa as the NW diameter increases from 20 to $\sim$80 nm. For NWs larger than $\sim$100 nm, no significant size effect was observed and the elastic modulus converged to the bulk value of 140 GPa. This result is consistent with the size effect reported in Chen et al.[7] Nonetheless, the measured values are slightly lower than those reported in ref 7 most likely because of the gradient-dominated field present in bending resonance tests.

Computationally, similar size dependence was predicted with the Young's modulus increasing from 169 to 194 GPa as NW diameters decreased from 20 to 5 nm. This size effect is attributed to surface reconstruction. Due to the long-range ionic interactions, the effect of surface reconstruction in ZnO NWs is quite different than the limited size effect observed in metallic nanowires.[30,31] In metals, the surfaces are usually in a tensile state of stress leading to overall contraction of the nanowire during relaxation. Hence, the effect of size on elastic properties like Young's modulus in metals is attributed to the intrinsic compressive state of the nanowire at equilibrium. Since a smaller metallic nanowire contracts more due to high surface to volume ratio, it has higher compressive strain at equilibrium and therefore a higher elastic modulus.[32] In the case of ZnO nanowires, the atomistic simulations predict the opposite behavior; that is, surfaces are initially in compression leading to an overall expansion of the nanowire upon relaxation. Surface atoms exhibit a much higher elastic modulus compared to inner atoms due to a smaller effective interatomic spacing caused by high radial contraction of the surface. Moreover, the atoms in the core of the wire do not exhibit bulk properties but rather a lower Young's modulus, depending on their radial position. The long-range surface effect in the case of ZnO nanowires can be attributed to long-range columbic interactions, which is different than the predicted behavior for metallic nanowires, where the surface effect dies out within $\sim$2 atomic layers. In summary, the size effect observed in ZnO nanowires is an outcome of surface relaxation together with long-range

interactions present in ionic crystals, which result in surfaces much stiffer than bulk. The high surface stiffness effect decays with decreasing surface to volume ratio, resulting in wires with diameter larger than ~100 nm exhibiting bulk behavior.

Acknowledgment. This work was supported by the National Science Foundation under Award Nos. CMMI - 0555734 and EEC − 0647560. We also acknowledge the grant by the Undergraduate Research Grant Program, administered by the Northwestern University Office of the Provost. We would also like to acknowledge Professor Diana Farkas from Virginia Tech University and Dr. Michael Baskes and Dr. S. G. Srivilliputhur from Los Alamos National Laboratories for insightful discussions. We also thank Dr. Shuyou Li for helping us with the TEM imaging and diffraction analyses. The authors acknowledge usage of the Electron Probe Instrumentation Center facilities at Northwestern University for experimental work and the BlueGene-L computational facility at Argonne National Laboratories.

Supporting Information Available: This material is available free of charge via the Internet at http://pubs.acs.org.

References

(1) Huang, M. H.; Mao, S.; Feick, H.; Yan, H.; Wu, Y.; Kind, H.; Weber, E.; Russo, R.; Yang, P. Room-Temperature Ultraviolet Nanowire Nanolasers. *Science* **2001**, *8*, 1897–1899.
(2) Gudiksen, M. K.; Lauhon, L. J.; Wang, J.; Smith, D. C.; Lieber, C. M. Growth of Nanowire Superlattice Structures for Nanoscale Photonics and Electronics. *Nature* **2002**, *415*, 617–619.
(3) Wang, Z. L.; Song, J. Piezoelectric Nanogenerators Based on Zinc Oxide Nanowire Arrays. *Science* **2006**, *312*, 242.
(4) Cui, Y.; Wei, Q.; Park, H.; Lieber, C. M. Nanowire Nanosensors for Highly Sensitive and Selective Detection of Biological and Chemical Species. *Science* **2001**, *293*, 1289–1291.
(5) Huang, Y.; Bai, X.; Zhang, Y. In Situ Mechanical Properties of Individual ZnO Nanowires and the Mass Measurement of Nanoparticles. *J. Physss: Condens. Matter* **2006**, *18*, L179–L184.
(6) Bai, X. D.; Gao, P. X.; Wang, G. L.; Wang, E. G. Dual-mode Mechanical Resonance of Individual ZnO Nanobelts. *Appl. Phys. Lett.* **2003**, *82* (26), 4806–4808.
(7) Chen, C. Q.; Shi, Y.; Zhang, Y. S.; Zhu, J.; Yan, Y. J. Size Dependence of Young's Modulus in ZnO Nanowires. *Phys. Rev. Lett.* **2006**, *96*, 075505.
(8) Ni, H.; Li, X. Young's Modulus of ZnO Nanobelts Measured using Atomic Force Microscopy and Nanoindentation Techniques. *Nanotechnology* **2006**, *17*, 3591–3597.
(9) Song, J.; Wang, X.; Riedo, E.; Wang, Z. L. Elastic Property of Vertically Aligned Nanowires. *Nano Lett.* **2005**, *5* (10), 1954–1958.
(10) Stan, G.; Ciobanu, C. V.; Parthangal, P. M.; Cook, R. F. Diameter-Dependent Radial and Tangential Elastic Moduli of ZnO Nanowires. *Nano Lett.* **2007**, *7*, 3691–3697.
(11) Simmons, G.; Wang, H. *Single Crystal Elastic Constants and Calculated Aggregate Properties*; MIT Press: Cambridge, MA, 1971.
(12) Desai, A. V.; Haque, M. A. Mechanical Properties of ZnO Nanowires. *Sens. Actuators, A* **2006**,
(13) Hoffmann, S,; Ostlund, F.; Michler, J.; Fan, H. J.; Zacharias, M.; Christiansen, S. H.; Ballif, C. Fracture Strength and Young's Modulus of ZnO Nanowires. *Nanotechnology* **2007**, *18*, 205503.
(14) Kulkarni, A. J.; Zhou, M.; Ke, F. J. Orientation and Size Dependence of the Elastic Properties of Zinc Oxide Nanobelts. *Nanotechnology* **2005**, *16*, 2749–2756.
(15) Wang, J.; Kulkarni, A. J.; Ke, F. J.; Bai, Y. L.; Zhou, M. Novel Mechanical Behavior of ZnO Nanorods. *Comput. Methods Appl. Mech. Eng.* **2008**, *197*, 3182–3189.
(16) Zhu, Y.; Moldovan, N.; Espinosa, H. D. A Microelectromechanical Load Sensor for In Situ Electron and X-ray Microscopy Tensile Testing of Nanostructures. *Appl. Phys. Lett.* **2005**, *86* (1), 013506.
(17) Zhu, Y.; Espinosa, H. D. An Electromechanical Material Testing System for In situ Electron Microscopy and Applications. *Proc. Natl. Acad. Sci. U.S.A.,* **2005**, *102* (41), 14503–14508.
(18) Espinosa, H. D.; Zhu, Y.; Moldovan, N. Design and Operation of a MEMS-Based Material Testing System for Nanomechanical Characterization. *J. Microelectromech. Syst.* **2007**, *16* (5), 1219–1231.
(19) Zhu, Y.; Corigliano, A.; Espinosa, H. D. A Thermal Actuator for Nanoscale In-situ Microscopy Testing: Design and Characterization. *J. Micromech. Microeng.* **2006**, *16*, 242–253.
(20) The device was initially calibrated to accurately determine the characteristics of the actuator and sensor. The thermal actuator exhibited a maximum displacement of about 1500 nm, which is well suited to prescribe deformation up to failure in 1D nanostructures. The load resolution of the differential capacitive sensor was about 12 nN, which is small enough to make accurate measurements of load.
(21) Yang, J.; Wang, W.; Ma, Y.; Wang, D. Z.; Steeves, D.; Kimball, B.; Ren, Z. F. High Throughput Growth of Zinc Oxide Nanowires From Zinc Powder with the Assistance of Sodium Chloride. *J. Nanosci. Nanotechnol.* **2006**, *6*, 2196–2199.
(22) The nanomanipulator probe is capable of movement increments as small as 1 nm and as large as 1 cm, which permits adequate manipulation of CNTs as well as quick translation within the SEM chamber.
(23) Peng, B.; Locascio, M.; Zapol, P.; Li, S.; Mielke, S.; Schatz, G.; Espinosa, H. D. Measurements of Near-Ultimate Strength for Multiwalled carbon nanotubes and Irradiation-induced crosslinking improvements. *Nat. Nanotechnol.*, advanced online publication, 2008.
(24) Plimpton, S. J. Fast Parallel Algorithms for Short-Range Molecular Dynamics. *J. Comput. Phys.* **1995**, *117*, 1–19.
(25) http://lammps.sandia.gov.
(26) Binks, D. J. *Computational Modeling of Zinc Oxide and related oxide ceramics, in Department of Chemistry*; University of Surrey: Harwell, England, 1994.
(27) Wolf, D.; Keblinski, P.; Phillpot, S. R.; Eggebrecht, J. Exact Method for the Simulation of Coulombic Systems by Spherically Truncated Pairwise r-1 Summation. *J. Chem. Phys.* **1999**, *110*, 8254.
(28) Yang, J.; Wang, W.; Ma, Y.; Wang, D. Z.; Steeves, D.; Kimball, B.; Ren, Z. F. High Through Growth of ZinC Oxide Nanowires from Zinc Powder with the Assistance of Sodium Chloride. *J. Nanosci. Nanotechnol.* **2006**, *6*, 2196–2199.
(29) Newnham, R. E. *Structure-Property Relations*; Springer-Verlag: New York, 1975.
(30) Diao, J. K.; Gall, K.; Dunn, M. L. Surface-Stress-Induced Phase Transformation in Metal Nanowires. *Nat. Mater.* **2003**, *2* (10), 656–660.
(31) Diao, J. K.; Gall, K.; Dunn, M. L. Surface Stress Driven Reorientation of Gold Nanowires. *Phys. Rev. B* **2004**, *70* (7), 075413.
(32) Kulkarni, R. A. J.; Zhou, M.; Qu, J. A Semi-Analytical Method for Quantifying the Size-Dependent Elasticity of Nanostructures. *Modell. Simul. Mater. Sci. Eng.* **2008**, *16*, 025002.

NL801724B